FULL PAPER

Applied Organometallic Chemistry WILEY

Improving enzymatic performance of antioxidant enzyme catalase in combination with [Mn (phen)₂Cl.H₂O]Cl.tu complex

Somaye Shahraki [ID] | Fereshteh Shiri [ID] | Zohreh Razmara [ID]

Department of Chemistry, University of Zabol, Zabol, Iran

Correspondence
Somaye Shahraki, Department of Chemistry, University of Zabol, Zabol, Iran.
Email: s-shahraki@uoz.ac.ir, somaye_shahraki@yahoo.com

Efforts to synthesize metal complexes that have good biological potency, such as anti-cancer or antioxidant properties, have expanded. In this study, an Mn complex containing 1,10-phenanthroline (phen) and thiourea (tu), [Mn (phen)₂Cl.H₂O]Cl.tu, was selected, and its interaction with the antioxidant enzyme bovine liver catalase (BLC) was evaluated by spectroscopic and molecular docking methods. Our results showed that Mn complex interacts with BLC via a dynamic, endothermic, entropy-driven mechanism. The binding constants (K_b) of BLC-Mn complex were 0.62 ± 0.01, 0.73 ± 0.03, and $2.62 \pm 0.09 \times 10^3$ M^{-1} at 303, 310, and 317 K, respectively. During complex interaction with catalase, the most important forces involved were hydrophobic forces. Considering that the quenching rate of tryptophan (Trp) was higher than that of tyrosine (Tyr), it can be concluded that Trp is closer to the Mn complex interaction site than Tyr. The CD spectra showed that the BLC secondary structure became more stable in the presence of the Mn complex and could be a reason for improving the catalytic activity of this enzyme. Molecular docking was used to predict that the Mn complex is able to bind to BLC and to identify specific residues. In general, the above Mn complex can be further evaluated as a suitable synthetic metallodrug due to its good antioxidant activity and binding function that improves the enzymatic activity of catalase.

KEYWORDS
antioxidant, catalase, interaction mechanism, Mn complexes, molecular docking

1 | INTRODUCTION

If oxygen molecules are incompletely reduced, reactive oxygen species, ROS (such as H_2O_2, $\bullet O_2^-$, $\bullet OH$, and $\bullet O_2^{-2}$), will be formed.[1] Increasing the level of them leads to significant damage, namely, oxidative stress.[2] Oxidative damage can have two reciprocal functions: It can damage healthy tissues and cells, and it can induce aging and cellular apoptosis, which can be used for anti-tumor and anti-bacterial properties. Therefore, proper regulation of ROS is a good way to treat redox-related

diseases. Redox enzymes play an important role in regulating the levels of ROS. One of the body's most important redox enzymes is catalase. This enzyme plays a key role in the decomposition of hydrogen peroxide in the body. Catalase protects cells from the harmful effects of this powerful oxidant by breaking down hydrogen peroxide into H_2O and O_2. The large (232 kDa) and tetrameric structure of this enzyme with four groups of heme containing iron facilitates the interaction of the enzyme with its substrate, H_2O_2.[3] Catalase inactivation has some side effects and can lead to diseases such as cancer, hypertension,

Parkinson's disease, malaria, and Alzheimer's disease.[4,5] In this enzyme, porphyrins are the active site for the substrate (H_2O_2). If catalase is inactivated and cannot break down the substrate, hydrogen peroxide accumulates in the cell, and ROS can lead to cell death.

Many drugs can affect catalase in terms of structure and catalytic activity. Therefore, the structural and functional study of biomacromolecule/drug systems is a very valuable field in biology and pharmacy. Investigating the interactions between drugs and large biomolecules can help to better understand the related mechanisms in the body and is also very useful for determining the effective concentration and toxicity of drugs. So far, many studies have been reported on the interaction of small molecules and catalase. Previous studies have shown that aspirin has a protective role on catalase function.[6] Palladium complex of [Pd (dach)(FIP)]$(NO_3)_2$ affects enzymatic activity as well as catalase structure, but overall, it cannot be considered as a serious catalase inhibitor.[7] Limited changes in the structure and function of catalase in interaction with other metal complexes are also observed.[2,8–10] Manganese is an element used in the structure of many biological molecules, such as enzymes. Interaction of Mn complexes with catalase has been less reported, although research has shown that manganese complexes are even capable of mimicking catalase activity.

Here, the effect of Mn complex, [Mn (phen)$_2$Cl.H_2O] Cl.tu,[11] where phen is 1,10-phenanthroline and tu is thiourea, on the catalytic performance and structure of bovine liver catalase (BLC) is evaluated using multispectroscopic methods, and a molecular docking simulation is used to explain the mode of binding. This complex was selected based on several important points: (i) Mn can participate in redox reactions in the body due to its redox abilities. (ii) Many Mn complexes as artificial enzymes are able to catalyze redox reactions such as the ROS deletion. (iii) In studying the biological abilities of Mn complex, its interaction with biomolecules, including enzymes, is very important. In this study, we attempt to focus on the impacts of a protentional antioxidant agent (Mn complex) on the catalytic performance and structure of important antioxidant enzyme, catalase.

2 | EXPERIMENTAL

2.1 | Materials and methods

The materials used in this research were purchased from Merck Co. (hydrogen peroxide 30%) and Sigma-Aldrich (BLC). In the study of catalytic performance of the enzyme, the concentration of the substrate (hydrogen peroxide) was estimated by spectroscopy at a wavelength of 240 nm with a quenching coefficient of 43.6 M^{-1} cm^{-1}.[12] Deionized water was used as a solvent to prepare the complex stock solution (5×10^{-3} M). Protein solution was prepared using Tris–HCl buffer, and its concentration was measured by UV–Vis spectrophotometer ($\varepsilon = 3.24 \times 10^5$ M^{-1} cm^{-1}).[3,12]

2.2 | Hirshfeld surface analysis

To gain more insight, better visualization of intermolecular interactions and to find out the 3D molecular surface analysis, the Hirshfeld surface distribution was performed.[13] Two-dimensional fingerprint analysis was performed to study molecular shapes and examine the exact percentage of all important intermolecular interactions.[14] For Mn complex, Hirshfeld surface analysis, as well as 2D fingerprint plots, and percentage of all important intermolecular contacts were generated by the Crystal Explorer Ver. 3.1 program package.[15] Both plots provide good qualitative and quantitative information for describing intermolecular interactions, such as short or long contacts and the strength of the intermolecular interactions by different colors and color intensity. The function normalized contact distance (d_{norm}) is a ratio enclosing the distances of the internal atom to any surface point (d_i), external (d_e) atom, and the van der Waals radii of the atoms.[16,17] d_i and de are unique identifier for each structure. However, when the intermolecular distances are close to van der Waals contacts, the d_{norm} will be equal to zero, which on the Hirshfeld surface presents by color of white. Two colors of blue and red indicate that the distances are longer and smaller than the sum of the corresponding van der Waals radii, respectively.

2.3 | DPPH scavenging activity

First, DPPH solution with a concentration of 40 mg L^{-1} was prepared. Then, a constant volume of Mn complex solution (0.1 ml) with concentrations ranging from 0–2,000 mg L^{-1} was added to 3.9 ml of radical solution in the dark. The solutions were stirred in the dark for 30 and 60 min. Then, the absorbance of the solutions was recorded at a wavelength of 517 nm. With the help of the following equation (Equation 1), the ability of the Mn complex to inhibit free radicals DPPH• can be estimated:

$$I\% = \frac{(A_0 - A_1)}{A_0} \times 100, \tag{1}$$

where A_0 and A_1 are the absorbance value of the control and the containing Mn complex solutions.

2.4 | Changes in catalase enzymatic activity

The substrate for the BLC is hydrogen peroxide. Catalase is able to break down this substrate into water and oxygen. Spectroscopy was used to measure the changes in the concentration of the substrate. For this purpose, a constant concentration of the H_2O_2 (1.0×10^{-2} M) is incubated (5 min) with a fixed amount of BLC (5.0×10^{-7} M), and its absorbance was recorded at 240 nm.[18] This experiment is then repeated in the presence of different concentrations of the Mn complex (0–5.0×10^{-5} M) to obtain the stoichiometric molar ratio of 1:0, 1:1, 1:5, 1:10, 1:25, 1:50, and 1:100. Effect of temperature (298, 308, 318, and 328 K) and incubation times (1, 24, and 48 h) on catalase activity was also studied in the presence or absence of Mn complex.[19]

2.5 | Fluorescence quenching

Agilent Cary Eclipse Fluorescence Spectrophotometer was applied to collect the fluorescence spectra. The studied wavelength range was selected between 300 and 500 nm. The experiments were done at $\lambda_{ex} = 285$ nm. A total of 5.0 nm was chosen for the width of the emission and excitation slit. In these experiments, to obtain suitable fluorescence intensity, the spectra were corrected for the inner filter effect.[20] We have done the fluorescence experiments at three temperatures of 303, 310, and 317 K. The fluorescence titrations performed in Tris–HCl buffer of pH 7.4, the amount of protein (5×10^{-6} M) was constant, and the concentration of Mn complex gradually increased (0–7.60×10^{-4} M). The incubation time was 5 min for each titration. The initial volume of the Tris–HCl buffer was 1,770 ml, and the volume of the catalase stock solution was 30 ml (the final volume of the initial solution without the presence of complex was 1,800 ml).

The Stern-Volmer equation (2) was used to analyze the fluorescence spectra (at $\lambda_{max} = 338$ nm)[21]:

$$\frac{F_0}{F} = 1 + K_{sv}[Q], \qquad (2)$$

where F_0 is free BLC fluorescence intensity and F is BLC fluorescence intensity after interaction with Mn complex. K_{SV} and [Q] are Stern–Volmer quenching constant and drug concentration, respectively. Graphs of F_0/F versus Mn complex concentration were plotted. The K_{SV} is obtained with the help of linear regression of this plot. According to the modified Stern–Volmer equation (Equation 2), the graphs of $\log(F_0 - F)/F$ versus log

[Mn complex] were also plotted and used to obtain the binding constant (K_b) and binding sites number (n)[22]:

$$\log \frac{F_0 - F}{F} = \log K_b + n\log[Q]. \qquad (3)$$

Thermodynamic parameters ($\Delta H°$, $\Delta S°$, and $\Delta G°$) were calculated using the following equations (Van't Hoff equation, Equation (4), and Gibbs–Helmholtz equation, Equation (5) to determine the type of Mn complex-BLC interaction[23,24]:

$$Ln\,K = -\frac{\Delta H°}{RT} + \frac{\Delta S°}{R}, \qquad (4)$$

$$\Delta G° = \Delta H° - T\Delta S°, \qquad (5)$$

Synchronous fluorescence measurements were done at the difference between the emission and excitation wavelengths ($\Delta\lambda$) values of 60 and 15 nm.

In fluorescence and UV–Vis experiments, dilution can have adverse effects on peak intensities. We diluted the working solution sufficiently to prevent this adverse effect.

2.6 | UV–vis absorption spectra

The UV–Vis spectra were obtained using a Jasco UV/Vis-7850 double-beam spectrophotometer. It has a quartz cell with a width of 1 cm. The wavelength range in these experiments was chosen between 200 and 450 nm. Mn complex concentrations ranged from 0 to 7.60×10^{-4} M, while a constant concentration of protein (5×10^{-6} M) was used. The incubation time of enzyme with the Mn complex was 3 min at each titration.

2.7 | Circular dichroism (CD) measurements

By a Jasco J-810 circular dichroism spectropolarimeter, the CD spectra of the free enzyme (5×10^{-6} M) and enzyme-Mn complex solutions with similar ratios (1:1) were recorded from 190 to 260 nm. In CD spectra, the baseline was corrected using subtracting the spectrum of the buffer solution. The secondary structure of the enzyme was calculated by CDNN software.

2.8 | Molecular docking simulation

To better understand in vitro relevant pharmacological interactions between the Mn complex and BLC,

computational docking has successfully been used. The crystal structure of BLC was retrieved from the Protein Data Bank (Code: 1TGU). BLC is a tetramer with four identical subunits, and each subunit contains a heme group in the active site. Because the active pocket is found inside each monomer, three chains from four identical sequences were removed. A purification process was performed by removing all heteroatoms and solvent molecules from the structure. Polar hydrogens were then added to BLC. The structure of Mn complex with CIF extension file (code: CCDC-2024904) has been downloaded from the Cambridge Crystallographic Data Center. Using Open Babel software, the CIF file of the Mn complex was converted to .pdb extension file. The grid box of $30 \times 18 \times 24$ Å was centered on Mn complex along the coordinates of the complex in X, Y, Z planes at 36.85, 38.70, and 25.61, with 1 Å grid spacing. The Mn complex was docked within the active site of BLC using the Smina program and the Lamarkian genetic algorithm.[25] The total number of runs was set at nine. The optimal docking was chosen based on the lowest binding free energy. In addition, Molegro Molecular Viewer 2.5 was used to calculate the interaction energy between the best pose of docked complex in to the catalase binding site and each amino acid.

2.9 | Calculation of accessible surface area

The accessible surface areas (ASAs) of BLC and BLC with Mn-complex were calculated using the NACCESS software (version 2.1.1), with the default settings.[26] This algorithm was first proposed by Lee and Richards.[27]

3 | RESULTS AND DISCUSSION

3.1 | Structure and Hirschfeld surface analysis

Molecular structure of Mn-complex is shown in Figure 1. As shown in the figure, the Mn (II) center achieves a slightly distorted octahedral geometry by coordination to four nitrogen atoms, one chlorine atom and one oxygen atom.[11] Mn complex has formed some hydrogen bonds between Cl counter ions and water oxygen atoms coordinated to the metal (Figure 2). These intermolecular hydrogen bonds in the complex structures increase the interaction between the Mn complex and catalase. Figure 3 exhibits the 3D d_{norm} surface that mapped over a fixed color scale of -0.53 (red) to 1.57 Å (blue) (3a) and 2D fingerprint (3b) with the main interactions of the

complex. In our complex, the concave red spots on the d_{norm} surfaces show strong interactions of O–H...O and O...H–O hydrogen bonds, which exhibited as acceptor spike (O...H) and donor spike (H...O) in the 2D fingerprint plot. The H...H interactions in 2D plot has the most significant contribution in the HS with 30.6% contribution. The C...H/H...C, Cl...H/H...Cl, H...N/N...H, C...S/S...H, and C...C contacts contribute to 24.3%, 16.4%, 9.75, 2.3%, and 8.5%, respectively.

3.2 | Antioxidant activity

Previous studies have shown that the potential of thiourea derivatives to inhibit free radicals and have antioxidant properties is very high.[28] DPPH• method was used to evaluate the antioxidant properties of the Mn complex (Figure 4). This method is based on the electron transfer process, in which the free radical DPPH• is stable and purple in room temperature but discolored after it reacts with the antioxidant. As can be seen, the antioxidant activity increases with increasing concentration of the Mn complex. DPPH radical scavenging activities of Mn complex at concentration of 100 mg L^{-1} is 61.1% and 65.2% after 30 and 60 min, respectively. Compared to many metal complexes, the Mn complex has more antioxidant activity. Due to the presence of thiourea and 1,10-phentanthroline ligands, this improvement in antioxidant activity was somewhat predictable.[29,30]

3.3 | Protective effect of the Mn complex on reducing enzyme performance

Enzyme activity was studied in the presence of Mn complex. In this study, several variables were examined: Mn complex concentration ($0-5 \times 10^{-5}$ M), incubation time (1, 24, and 48 h), and temperature (298, 308, 318, and 328 K). To investigate the effect of Mn complex concentration on enzyme activity, a constant amount of BLC was incubated with different concentrations of Mn complex ($0-5 \times 10^{-5}$ M) for 1 h. After 1 h, no significant change in enzyme activity was observed (Figure 5a). However, if catalase is incubated in Tris buffers for a long time (24 and 48 h), its activity will be reduced to some extent (27.4% after 24 h and 33.1% after 48 h). Interestingly, catalase activity was significantly protected in the presence of the Mn complex (Figure 5a). This protection is greater at high concentrations; for example, when the Mn complex concentration is 5×10^{-5} M, it improves catalase activity by 5.06% after 24 h and by 4.81% after 48 h. Enzyme activity at different temperatures was also examined. As shown in the Figure 5b, with increasing

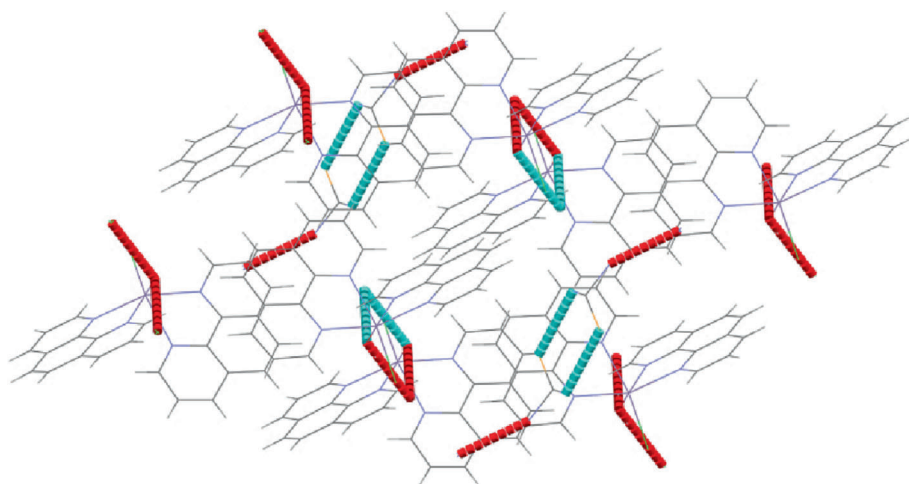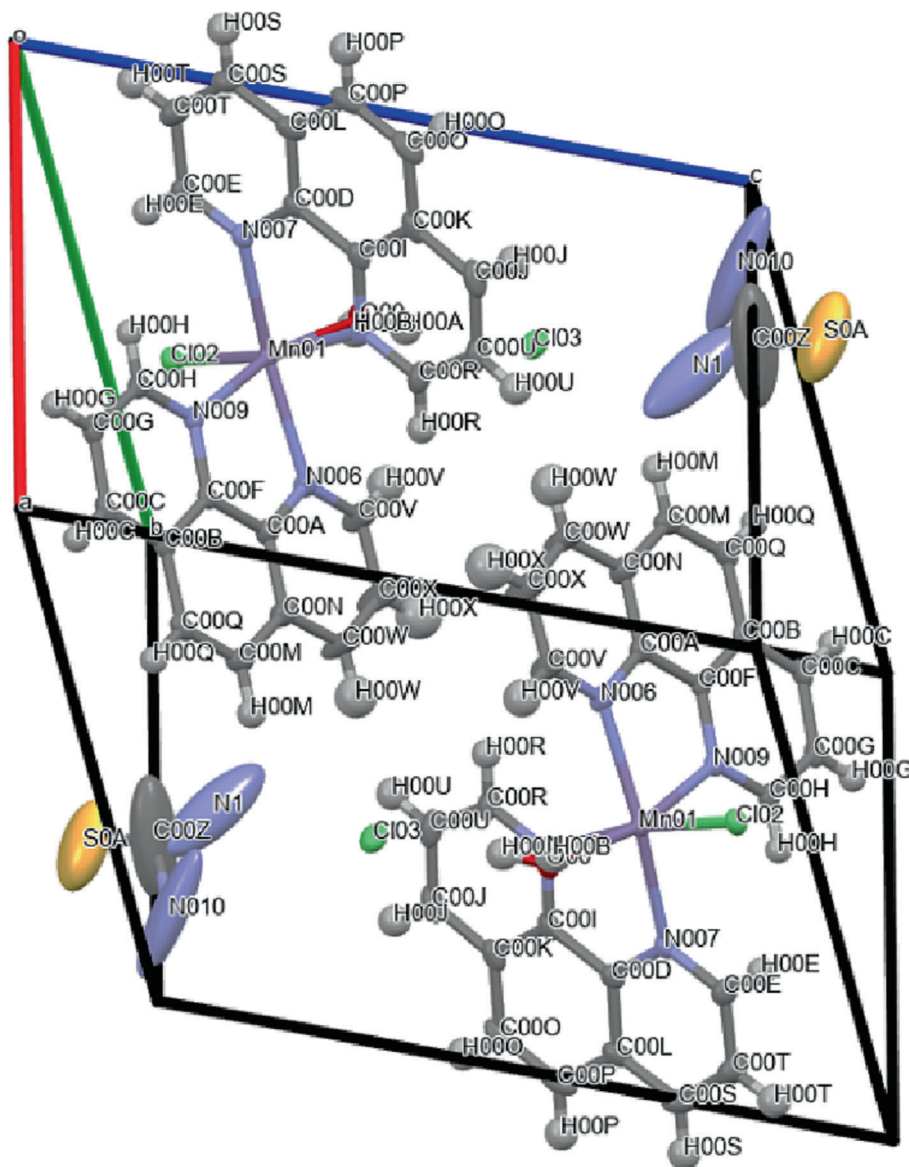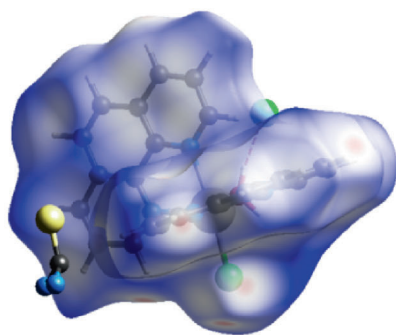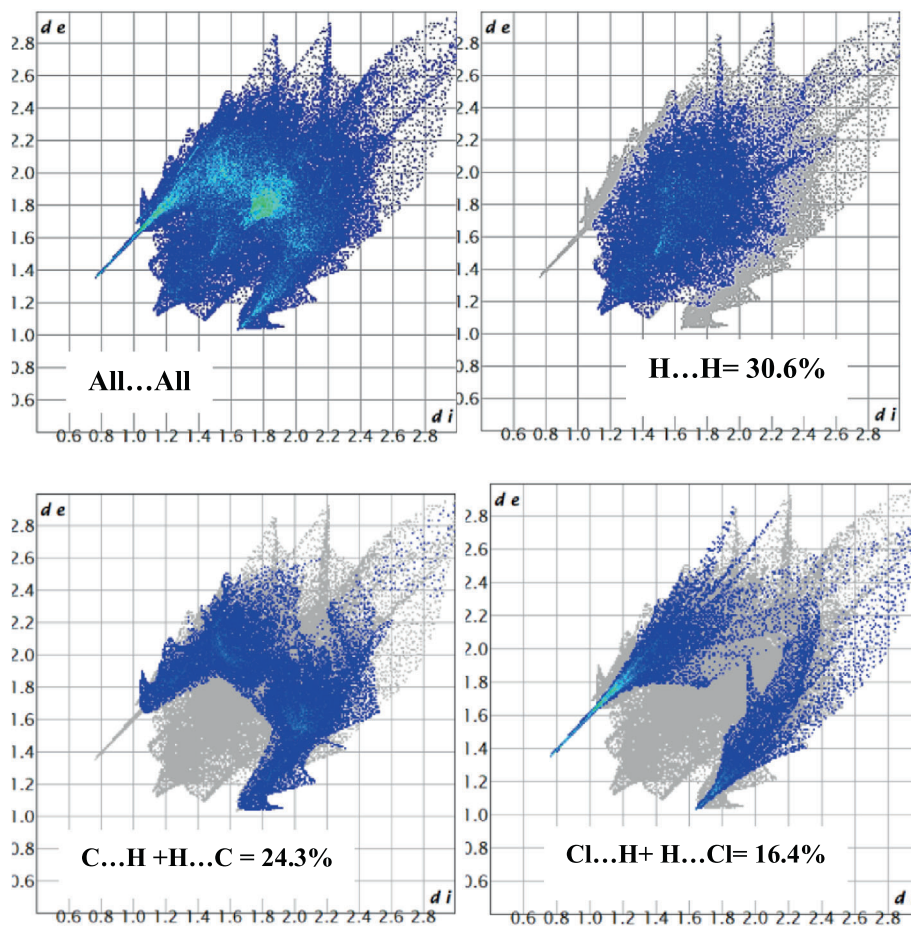**FIGURE 1** Atomic numbering in the molecular structure of Mn complex.

FIGURE 2 Hydrogen bonds in Mn complex presented as blue and red dashed lines.

(a)

(b)

FIGURE 3 The Hirshfeld surface for Mn complex by dnorm function (range −0.53, red, and 1.57, blue) (a); the 2D fingerprint of complex (b).

temperature from 298 to 328 K, the catalytic activity decreases significantly. Interestingly, if this experiment is repeated in the presence of the Mn complex (0–5 × 10^{-5} M), the catalytic activity is somewhat improved. The decrease in catalase activity with increasing temperature is quite predictable, because the protein structure loses its stability with increasing temperature. However, the presence of the Mn complex along with the enzyme has somewhat improved catalytic activity. Protective effects for other molecules such as well-known anti-malarial drug Artemisinin (ART) and Aspirin have also been previously reported.[3,6]

3.4 | Fluorescence quenching analysis

Some techniques can be used to study the structural changes of proteins and inner fluorophores. One of the most important methods is fluorescence.[31] In most proteins, the main cause of fluorescence emission is the two
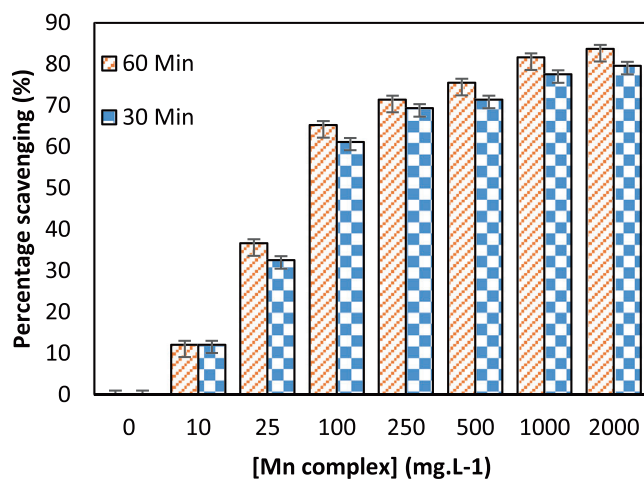
https://www.tarjomano.com

FIGURE 4 Antioxidant activity of Mn complex by DPPH method after 30 and 60 min.

FIGURE 6 The BLC fluorescence spectra (5×10^{-6} M) before and after interaction with various amounts of Mn complex. [Mn complex] = $0-7.60 \times 10^{-4}$ M.
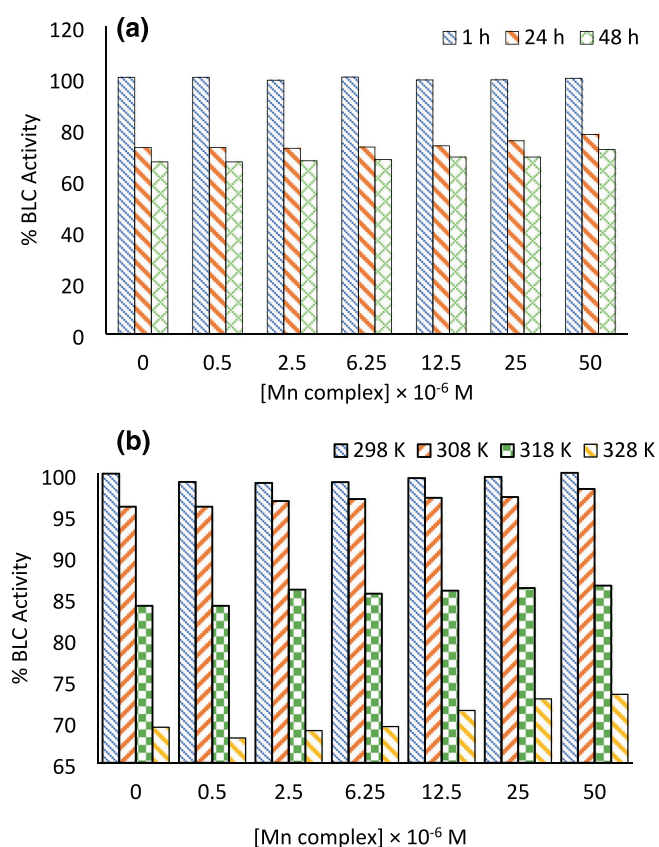

FIGURE 5 BLC catalytic performance at different (a) incubation times (1, 24, and 48 h) and (b) temperatures (298, 308, 318, and 328 K) in the presence of Mn complex ($0-5.0 \times 10^{-5}$ M).

amino acids Trp and Tyr. Binding of small molecules to proteins can quench the fluorescence emission. Therefore, with the help of this important technique, the mechanism of ligand interaction with protein can be evaluated, as well as some structural changes in
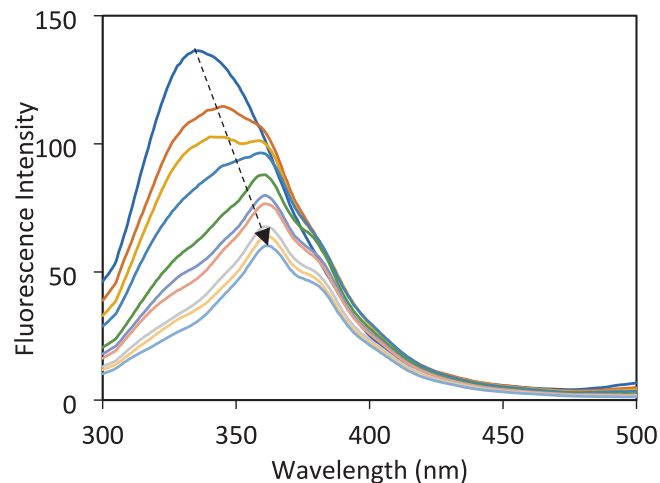
protein.[32] To investigate the mechanism of Mn complex interaction with BLC, catalase titration test was performed by different concentrations of Mn complex ($0-7.60 \times 10^{-4}$ M) using fluorescence emission at three temperatures of 303, 310, and 317 K, emission region of 300–500 nm, and excitation wavelength of 285 nm (maximum emission wavelength was 338 nm) (Figure 6). As can be seen, with increasing the Mn complex to the BLC solution, the intensity of enzyme fluorescence emission decreases, and at higher concentrations, in addition to the red shift (from 338 to 361 nm), the peak structure changes to some extent (the Mn complex did not show emission in this region), which confirms the structural changes of the BLC during interaction with Mn complex.

To explain the quenching of the fluorescence emission intensity of protein during interaction with ligand, various mechanisms have been proposed, including static and dynamic mechanisms. The type of mechanism can be easily predicted because the interaction process is completely temperature dependent. For this purpose, fluorescence data are analyzed by Stern–Volmer equation (Equation 2). The calculated parameters (K_{SV}, Stern–Volmer quenching constant, and k_q, quenching rate constant) as well as fitting plots at three different temperatures are shown in Table 1 and Figure 7a, respectively. The results of Table 1 show that with increasing temperature, the values of K_{SV} increase. The direct relationship between the K_{SV} and the temperature confirms the dynamic collision plays an important role during the interaction of Mn complex and enzyme. Furthermore, the quenching constant k_q is close to the maximum scattering collision quenching constant (2×10^{10} L·mol^{-1}·s^{-1}), indicating that Mn complex quenches the BLC fluorescence by a dynamic mechanism.[33]

TABLE 1 The obtained parameters in the Mn complex-BLC system.

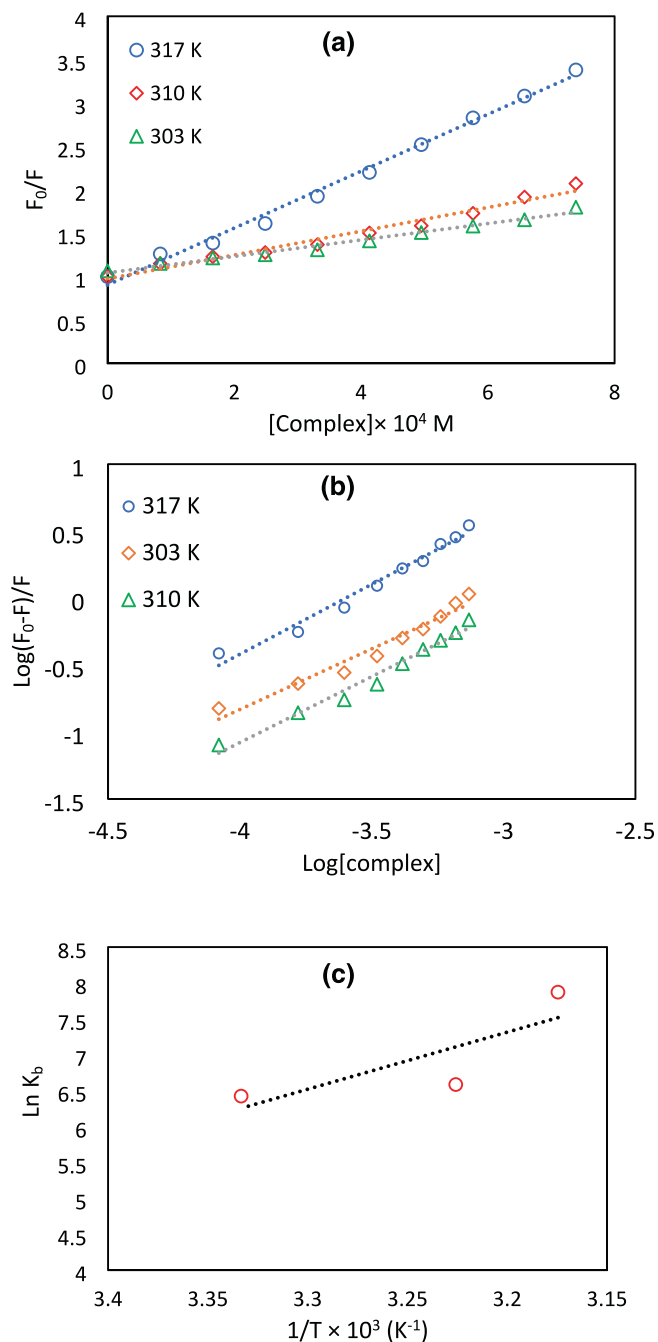| T(K)	n	$K_{SV}(\times 10^2 \text{ M}^{-1})$	k_q $(\times 10^{10} \text{ M}^{-1})$	K_b $(\text{M}^{-1} \times 10^3)$	$\Delta G°(\text{kJ mol}^{-1})$	$\Delta H°(\text{kJ mol}^{-1})$	$\Delta S°(\text{kJ mol}^{-1} \text{ K}^{-1})$
303	0.91 ± 0.02	9.46 ± 0.41	9.46 ± 0.41	0.62 ± 0.01	-35.26	66.30	0.27
310	0.98 ± 0.02	13.7 ± 1.71	13.7 ± 1.71	0.73 ± 0.03	-32.27		
317	1.04 ± 0.03	38.9 ± 3.11	38.9 ± 3.11	2.62 ± 0.09	-29.30		

FIGURE 7 (a) The Stern–Volmer quenching plots of BLC before and after interaction with various amounts of Mn complex at three temperatures. (b) The plot of log (F$_0$-F/F) versus log [Mn complex] for BLC-Mn complex system at three temperatures. (c) Plots of Ln$_{Kb}$ versus 1/T for Mn complex–BLC system.

3.5 | Binding and thermodynamic parameters

Many papers have reported binding constant of BLC after interactions with small molecules by using modified Stern–Volmer equation (3). In this study, binding constant (K_b) and n (Table 1) were calculated from plot of log(F$_0$-F)/F versus log[Mn complex] (Figure 7b) at three temperatures (303, 310, and 317 K) when λ_{ex} = 285 nm. As can be seen in Table 1, n values were obtained close to 1 at three temperatures, indicating that the protein can only bind to the Mn complex through one binding site. In fact, increasing concentration or temperature change does not activate other binding sites of BLC for Mn complex interaction. On the other hand, the K_b values were in the order of magnitude of 10^3 M^{-1}. The interaction strength between small molecules and proteins is important in biological studies. The above results indicate that Mn complex deserved a moderate binding affinity in BLC. The binding constant (K_b) values were obtained 0.62 ± 0.01, 0.73 ± 0.03, and $2.62 \pm 0.09 \times 10^3$ M^{-1} for Mn complex-BLC system at three temperatures from 303 to 317 K. The Mn complex's tendency to BLC is increased at higher temperatures. Therefore, the interaction process is temperature dependent and endothermic. This Mn complex-temperature behavior justifies the dynamic mechanism and confirms Stern-Volmer's results. In the following, we will study the thermodynamic parameters.

Different forces can participate in the binding of protein and ligands. One of the best ways to estimate the type of forces involved in the interaction process is to study thermodynamic parameters (entropy changes, $\Delta S°$; enthalpy changes, $\Delta H°$). These forces are non-covalent and include hydrogen bonds, van der Waals forces, and hydrophobic and electrostatic interactions. Predicting the type of interaction in ligand-protein interaction is possible by sign of these parameters.[18,34] Accordingly, thermodynamic parameters ($\Delta S°$, $\Delta H°$, and $\Delta G°$, Gibbs free energy) were calculated using Equations (4) and (5) and the plot of K_b versus T^{-1} (Figure 7c). The Mn complex interaction with BLC is a spontaneous process because $\Delta G° < 0$. The $\Delta H° > 0$ indicates interaction process in Mn complex-BLC system is an endothermic process. The

Mn complex-BLC interaction process is entropy-driven, spontaneous, and endothermic.[33] In addition, the positive sign of entropy and enthalpy changes confirms that the most important forces in the Mn complex-BLC interaction process are hydrophobic interactions. Given the presence of phenanthroline ligand in the structure of the Mn complex, such an interaction is predictable. This observation also showed good agreement with the docking and modeling results.

3.6 | Conformational changes of BLC

Various methods can be used to evaluate the conformational changes of proteins caused by ligand interactions. In this research, synchronous and 3D fluorescence, UV–Vis, and CD spectra have been used.

One of the valuable techniques in investigating the microenvironment around fluorophores (Trp and Tyr) is synchronous fluorescence spectroscopy. This information is obtained when the wavelength interval ($\Delta\lambda$) between the excitation and emission wavelengths are 15 nm (for tyrosine) and 60 nm (for tryptophan). In synchronous spectrum, if the polarity of the environment around the chromophore changes, it will lead to the shift in the λ_{max}. Previous studies have shown that chromophores are more exposed to polar solvents; the λ_{max} will have a red shift, but if the amino acid is buried in a hydrophilic cavity, the λ_{max} shift is towards shorter wavelengths (blue shift).[35–37] Accordingly, to evaluate microenvironmental changes near tyrosine and tryptophan, the synchronous fluorescence spectrum of catalase was recorded. Figure 8 presents the synchronous fluorescence spectra of catalase at λ = 60 nm (for Trp) and 15 nm (for Tyr). As can be seen from Figure 8, the intensity of fluorescence emission decreases in both fluorophores in the presence of different concentrations of the Mn complex, but in the case of Trp, the λ_{max} is shifted to shorter wavelengths (from 289 to 278 nm, blue shift). These results showed that Trp microenvironment was affected during the interaction of Mn complex and BLC.[38]

When the emission of catalase is recorded at different excitation wavelengths (from 200 to 350 nm), a three-dimensional fluorescence spectrum including emission, excitation, and intensity can be achieved. Figure 9 is related to the 3D fluorescence spectrum of catalase before and after interaction with Mn complex. Peak A ($\lambda_{em} = \lambda_{ex}$) is the first-order Rayleigh scattering, and B ($\lambda_{em} = 2\lambda_{ex}$) is the second-order Rayleigh scattering. After interaction with Mn complex, the intensity of these two peaks has decreased. Peak 1 (λ_{ex} = 280 nm, λ_{em} = 330 nm) is the characteristic peak of Tyr, Trp, and Phe; peak 2 mainly related to the fluorescence changes of the polypeptide backbone.[39] As can be seen, in addition
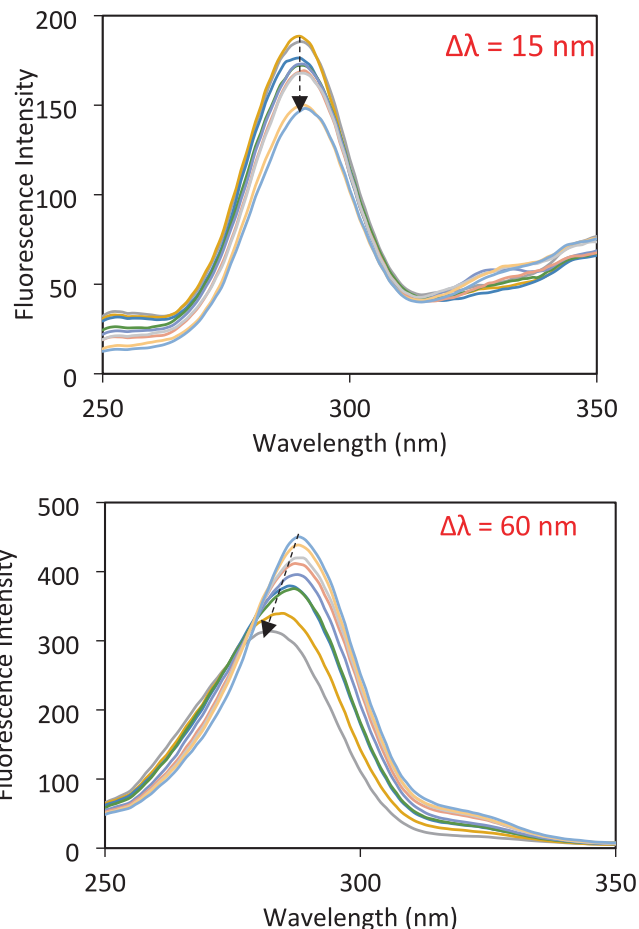

FIGURE 8 The BLC synchronous fluorescence spectra before and after interaction with various values of Mn complex [BLC] = 5×10^{-6} M and [Mn complex] = 0–5.2×10^{-4} M.

to the decrease in intensity, peaks 1 and 2 have also shown a shift in the maximum wavelength. Such observations could be a reason for the unfolding of the BLC backbone after interaction with the Mn complex and would also confirm the UV–Vis results.

The structural changes of proteins can also be studied with the help of UV–Vis spectroscopy. Figure 10a shows the UV–Vis spectrum of the BLC in the absence and presence of Mn complex. In general, the UV–Vis spectrum of proteins shows two main adsorption bands, a strong adsorption in the 210 nm regions that reflects the structure of the protein polypeptide backbone and a weak adsorption in the 278 nm region that reflects the change in chromophore microenvironment. By adding the Mn complex to the BLC solution, the intensity of the absorption peak around 210 and 278 nm gradually increased. This denoted that the interaction between Mn complex and BLC led to a change in the protein spatial structure.[40]

Another sensitive and useful technique, CD spectroscopy, can be used to study changes in the protein secondary structure. Accordingly, a constant concentration of BLC (5×10^{-6} M) was incubated by the Mn complex
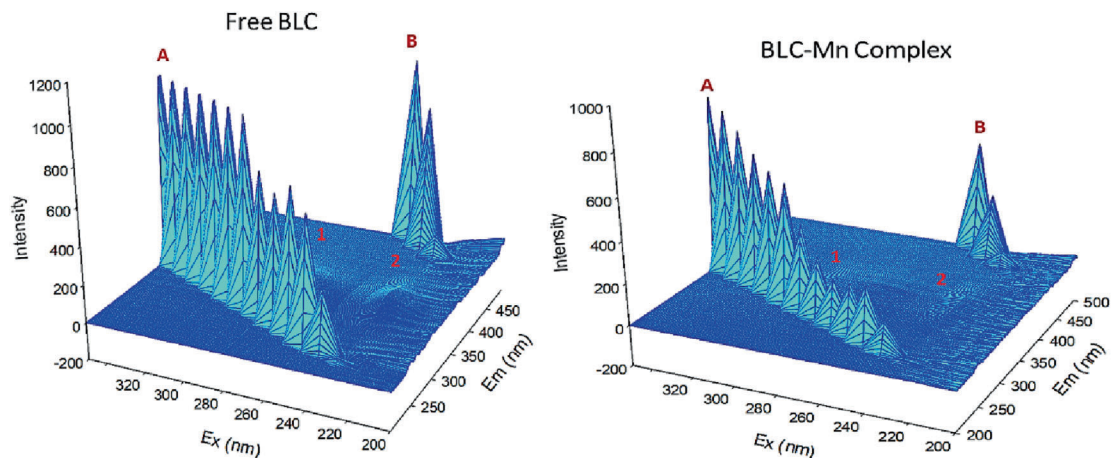
WILEY Applied Organometallic Chemistry

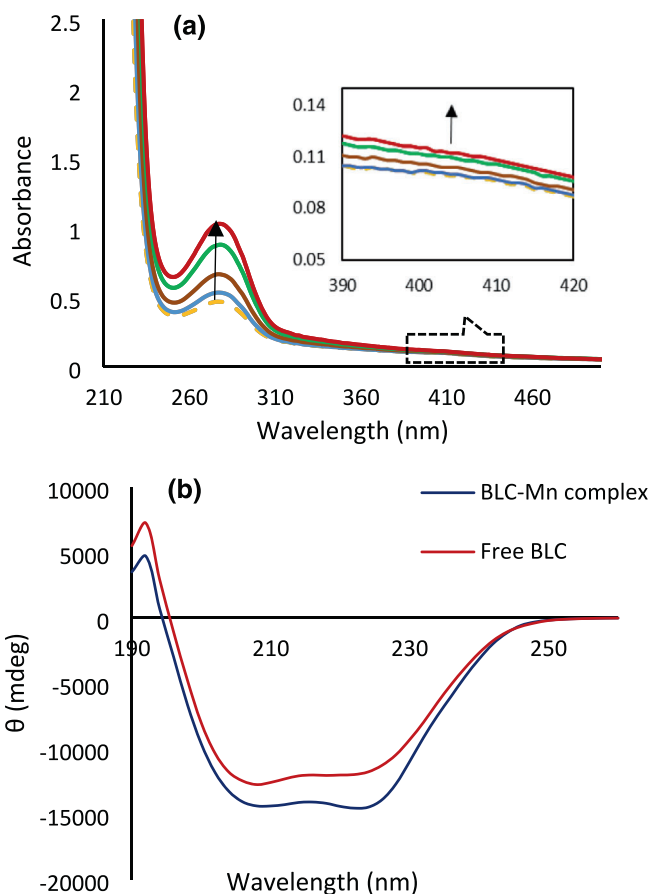**FIGURE 9** Three-dimensional fluorescence. Free BLC and Mn complex-BLC systems.

FIGURE 10 (a) BLC absorption spectrum; before (dash line) and after interaction with various amounts of Mn complex (solid lines). [BLC] = 5×10^{-6} M; [Mn complex] = $0-7.60 \times 10^{-4}$ M. (b) CD spectra of BLC before and after interaction with various amounts of Mn complex. [BLC] = [Mn complex] = 5×10^{-6} M.

TABLE 2 The content of BLC secondary structure before and after interaction with Mn complex.

System	Secondary structure in BLC (%)		
	α helix	β sheet	Random coil
BLC	21.6	25.2	31.3
BLC-Mn Complex	23. 9	27.5	33.7
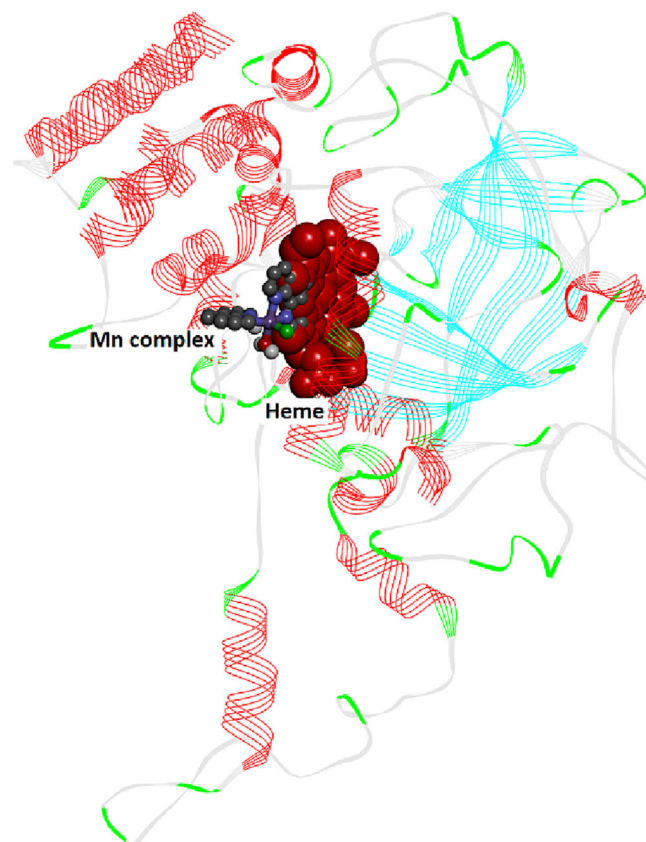
FIGURE 11 Molecular structure of BLC (1tgu pdb code) and binding sites of Mn complex on BLC.

(5×10^{-6} M) for 3 min. Catalase has a negative spectrum in the range of 190 to 260 nm, and, as shown in Figure 10b, its intensity decreases in the presence of the

SHAHRAKI ET AL.

Mn complex. CDNN program can be used to analyze the obtained CD spectra and predict the secondary structures of the BLC before and after the interaction with the Mn complex. As can be seen from Table 2, the hydrogen bonding network of the BLC and its secondary structure are strengthened to a limited extent during the interaction. This result could possibly be a reason for improving the catalytic activity of catalase. That is, although catalase has undergone structural changes during drug interactions, these changes have somewhat facilitated the entry of the substrate into the active site.

3.7 | Molecular docking of BLC-Mn complex

To study the interaction between the studied Mn complex and amino acids in the enzyme cavity, molecular docking

was used. Mn complex makes a favorable interaction profile in the cavity of BLC by binding directly to the active site and the heme group (Figure 11). The binding affinity of BLC and the most favorable conformation of the Mn complex was -10.13 kcal mol^{-1}. Smina's binding affinity for all conformers is shown in Table 3. The following amino acid residues in the BLC cavity surround the Mn complex with hydrophobic interactions: VAL72, ALA157, PHE160, PRO161, ILE164, HIS165, ARG353, ALA356, and TYR357 (Figure 12a). Based on the hydrophobicity of the receptor residues, the surface area shown in Figure 12b is colored from the blue for hydrophilic to

TABLE 3 Various conformers of Mn complex (BLC Smina score).

Pose	Affinity of Mn complex (kcal mol^{-1})
1	-10.13
2	-9.86956
3	-8.87171
4	-8.70488
5	-8.47458
6	-8.4612
7	-8.32348
8	-8.30819
9	-8.2412

TABLE 4 Molecular docking results: energy of interaction between the Mn complex and BLC-responsive amino acid.

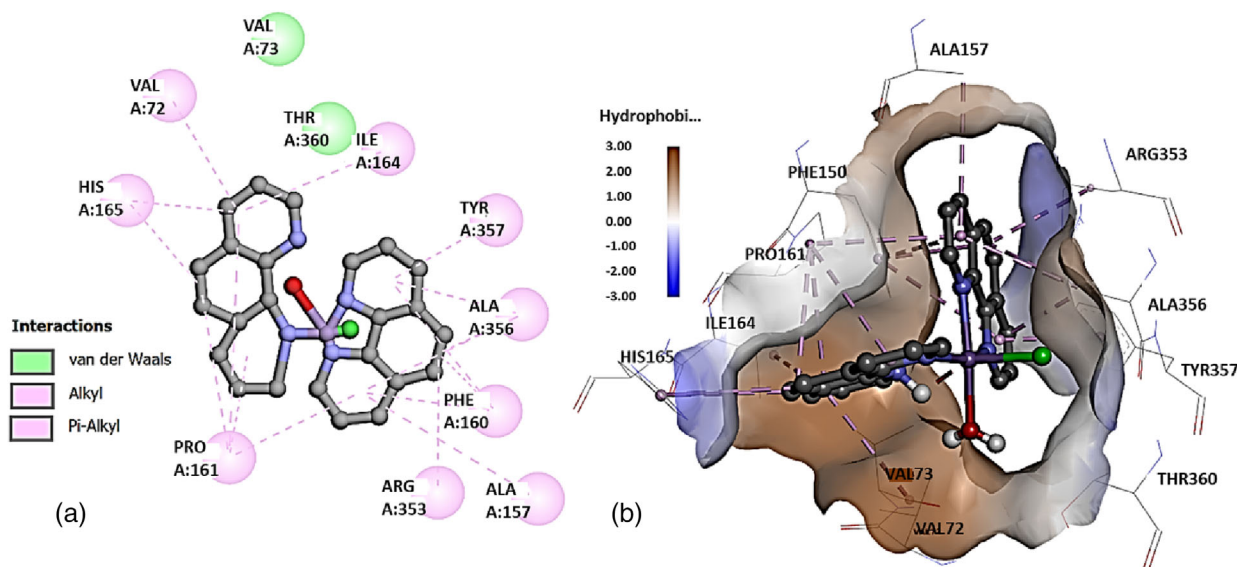| Amino acid residues	Interaction energykJ mol^{-1}
Ala157	-4.63213
Ala356	-12.7078
Arg353	-4.7704
Asp359	-1.15681
Gly352	-2.99085
His165	-5.4816
Ile164	-3.91244
Phe160	-27.2321
Phe355	-0.41079
Pro161	-24.0401
Thr360	-4.20795
Tyr357	-11.5383
Val72	-9.18309
Val73	-2.06225

FIGURE 12 BIOVIA Discovery Studio Visualizer showing the important interacting residues of BLC with Mn complex (a) 2D and (b) 3D.

WILEY Applied Organometallic Chemistry

SHAHRAKI ET AL.

Residues	ASA ($\mathring{A}^2$) of BLC	ASA ($\mathring{A}^2$) of BLC with Mn complex	ΔASA ($\mathring{A}^2$)
VAL72	69.8	38.4	31.4
ALA157	30.5	14	16.5
PHE160	30.8	7.2	23.6
PRO161	55.9	17.7	38.2
ILE164	6.1	1.6	4.5
HIS165	68.4	54.8	13.6
ARG353	16.9	11.2	5.7
ALA356	40.1	0	40.1
TYR357	32.7	15.8	16.9

TABLE 5 The ASA ($\mathring{A}^2$) values of the important active site residues of free BLC and BLC-Mn complex and changes in the ΔASA ($\mathring{A}^2$).

brown for hydrophobic. Hydrophobic interactions play a significant role in determining the Mn complex and BLC binding affinity; however, VAL73 and THR 360 are van der Waals interactions with the Mn complex. This indicates that the docking results obtained are validated by fluorescence quenching. In Table 4, the interaction energies between the Mn complex and the amino acid residues in the active site of catalase are presented.

3.8 | Variations in BLC's ASA

Surface residues provide information on possible active sites. By comparing the ASA of a free protein to that complexed with an inhibitor, the packing of residues within a protein structure or their significance to ligand binding can be determined. ASA changes (ΔASA, $\mathring{A}^2$) of free BLC and BLC-Mn complex are listed in Table 5. The total ASA of BLC and BLC-Mn complex were 26,000.3 and 25,822.5 $\mathring{A}^2$, respectively. As a consequence of this great reduction in ASA, it is evident that Mn complex binding to BLC is effective. An interaction is viewed as very active, if during the transition from the free to the complexed state, a residue loses at least 10 $\mathring{A}^2$ of its ASA.[41] From Table 5, it can be seen that most residues lose more than 10 of ASA ($\mathring{A}^2$) after binding to the Mn complex. These are VAL72, ALA157, PHE160, PRO161, HIS165, ALA356, and TYR357, which have a large effect in micro-environment of BLC. Only two residues, ILE164 and ARG353, lost 4.5 and 5.7 ASA ($\mathring{A}^2$), respectively. So this finding is the same phenomenon as the fluorescence quenching of BLC caused by Mn complex.

4 | CONCLUSION

One of the beneficial elements that is also used in the structure of some metalloenzymes is manganese. Due to its special properties, including its redox potential, Mn

complexes have been considered by researchers, especially in design of artificial enzyme.[42] Before using them in medical cases, their interaction with biological molecules seems necessary. Here, a Mn complex containing 1,10-phenanthroline and thiourea was selected, and its antioxidant activity was investigated by DPPH•. The above Mn complex showed a greater ability to inhibit free radical DPPH• compared to many metal complexes. The fluorescence data revealed that Mn complex could quench BLC with dynamic quenching mechanism. Synchronous fluorescence analysis indicated that the Trp residue of BLC had a bolder role in quenching and interacting with Mn complex. The analysis of Stern–Volmer plots showed that interaction process has negative ΔG° values and positive ΔH° and ΔS° values. So, in agreement with the docking, hydrophobic forces predominate in the interaction process. The CD data indicated a slight change in the secondary structure of BLC in the presence of Mn complex. Overall, this study showed the Mn complex interacts with the BLC with moderate potency and the interaction leads to greater stability of the secondary structure of the catalase and subsequently improves its catalytic activity.

AUTHOR CONTRIBUTIONS
Somaye Shahraki: Conceptualization; funding acquisition; project administration; supervision; writing—review and editing.

ORCID
Somaye Shahraki https://orcid.org/0000-0002-0597-4459
Fereshteh Shiri https://orcid.org/0000-0003-2879-9347
Zohreh Razmara https://orcid.org/0000-0001-6780-1169

REFERENCES

[1] H. Zhao, R. Zhang, X. Yan, K. Fan, *J. Mater. Chem. B* **2021**, *9*(35), 6939.

[2] S. Shahraki, M. Saeidifar, H. S. Delarami, H. Kazemzadeh, *J. Mol. Struct.* **2020**, *1205*, 127590.

[3] R. R. Samal, K. Kumari, Y. Sahoo, S. K. Mishra, U. Subudhi, *Int. J. Biol. Macromol.* **2021**, *172*, 418.

[4] L. Góth, P. Rass, A. Páy, *Mol Diagn* **2004**, *8*(3), 141.

[5] A. Escribano, M. Amor, S. Pastor, S. Castillo, F. Sanz, P. Codoñer-Franch, F. Dasí, *Thorax* **2015**, *70*(1), 82.

[6] B. Koohshekan, A. Divsalar, M. Saiedifar, A. A. Saboury, B. Ghalandari, A. Gholamian, A. Seyedarabi, *J. Mol. Liq.* **2016**, *218*, 8.

[7] R. Ghobadi, A. Divsalar, A. R. Harifi-Mood, A. A. Saboury, M. Eslami-Moghadam, *J. Photochem. Photobiol., a* **2018**, *364*, 288.

[8] S. Shahraki, H. S. Delarami, M. Saeidifar, *J. Mol. Liq.* **2019**, *287*, 111003.

[9] S. Shahraki, Z. Razmara, F. Shiri, *J. Mol. Struct.* **2020**, *1208*, 127865.

[10] S. Shahraki, H. S. Delarami, M. Saeidifar, R. Nejat, *Int. J. Biol. Macromol.* **2020**, *152*, 126.

[11] Z. Razmara, M. Kubicki, *J. Mol. Struct.* **2021**, *1234*, 130143.

[12] S. Rashtbari, G. Dehghan, R. Yekta, A. Jouyban, M. Iranshahi, *Adv. Pharm. Bull.* **2017**, *7*(3), 349.

[13] M. A. Spackman, D. Jayatilaka, *CrystEngComm* **2009**, *11*(1), 19.

[14] J. J. McKinnon, M. A. Spackman, A. S. Mitchell, *Acta Crystallogr., Sect. B: Struct. Sci.* **2004**, *60*(6), 627.

[15] S. Wolff, D. J. Grimwood, J. J. McKinnon, M. J. Turner, D. Jayatilaka, M. A. Spackman, *Crystal Explorer*, University of Western Australia Crawley, Australia **2012**.

[16] J. J. McKinnon, A. S. Mitchell, M. A. Spackman, *Chem.–A Eur. J.* **1998**, *4*(11), 2136.

[17] J. J. McKinnon, D. Jayatilaka, M. A. Spackman, *Chem. Commun.* **2007**, *37*, 3814.

[18] P. D. Ross, S. Subramanian, *Biochemistry* **1981**, *20*(11), 3096.

[19] L. Chen, J. Zhang, Y. Zhu, Y. Zhang, *Food Chem.* **2018**, *244*, 378.

[20] J. R. Lakowicz, *Principles of Fluorescence Spectroscopy*, Springer Science & Business Media **2013**.

[21] M. R. Eftink, C. A. Ghiron, *Anal. Biochem.* **1981**, *114*(2), 199.

[22] M. Makarska-Bialokoz, *Spectrochim. Acta, Part a* **2018**, *193*, 23.

[23] T. Madrakian, H. Bagheri, A. Afkhami, M. Soleimani, *J. Lumin.* **2014**, *155*, 218.

[24] J. W. Gibbs, A method of geometrical representation of the thermodynamic properties by means of surfaces. The Collected Works of J. Willard Gibbs, Ph. D., LL. D, **1957**: p. 33–54.

[25] D. R. Koes, M. P. Baumgartner, C. J. Camacho, *J. Chem. Inf. Model.* **2013**, *53*(8), 1893.

[26] S. J. Hubbard, J. M. Thornton, NACCESS. Computer Program, Department of Biochemistry and Molecular Biology, University College London. 2(1), **1993**.

[27] B. Lee, F. M. Richards, *J. Mol. Biol.* **1971**, *55*(3), 379-IN4.

[28] D. Q. Huong, M. van Bay, P. C. Nam, *J. Mol. Liq.* **2021**, *340*, 117149.

[29] H. Nouri, H. Mansouri-Torshizi, S. Shahraki, *J. Iran. Chem. Soc.* **2021**, *18*(12), 3281.

[30] S. Shahraki, H. Samareh Delarami, H. Mansouri-Torshizi, H. Nouri, *J. Mol. Liq.* **2021**, *334*, 116527.

[31] A. Zare Karizak, A. Divsalar, A. Leilabadi Asl, F. Fateminasab, S. Shityakov, A. A. Saboury, *Spectrochim. Acta, Part a* **2022**, *267*, 120538.

[32] F. Mohammadnia, M. Fatemi, S. Taghizadeh, *Luminescence* **2020**, *35*(2), 266.

[33] J. Zhang, L. Chen, Y. Zhu, Y. Zhang, *Food Chem.* **2020**, *309*, 125743.

[34] F. Liu, Y. Zhang, Q. Yu, Y. Shen, Z. Zheng, J. Cheng, W. Zhang, Y. Ye, *Food Chem. Toxicol.* **2019**, *134*, 110867.

[35] Y. Teng, H. Zhang, R. Liu, *Mol. BioSyst.* **2011**, *7*(11), 3157.

[36] A. Varlan, M. Hillebrand, *Molecules* **2010**, *15*(6), 3905.

[37] Y. Wang, G. Zhang, J. Pan, D. Gong, *J. Agric. Food Chem.* **2015**, *63*(2), 526.

[38] J. Jayabharathi, K. Jayamoorthy, V. Thanikachalam, R. Sathishkumar, *Spectrochim. Acta, Part a* **2013**, *108*, 146.

[39] M. Huo, L. Zhao, T. Wang, W. Zong, R. Liu, *J. Mol. Recognit.* **2020**, *33*(3), e2822.

[40] T. Niu, X. Zhu, D. Zhao, H. Li, P. Yan, L. Zhao, W. Zhang, P. Zhao, B. Mao, *Spectrochim. Acta, Part a* **2023**, *285*, 121871.

[41] B. K. Sahoo, K. S. Ghosh, S. Dasgupta, *Biopolym.: Orig. Res. Biomol.* **2009**, *91*(2), 108.

[42] S. Shahraki, *Colloids Surf. B: Biointerf.* **2022**, *218*, 112727.